Comparison of Ultrasonic Pole Figures Based upon Ultrasonic Nondestructive Evaluation Method with Pole Figures Based upon Finite Element Polycrystal Model*

Shihua TANG** and Michiaki KOBAYASHI**

The ultrasonic wave velocities in a polycrystalline aggregate are sensitively influenced by texture changes due to plastic deformation, and their relationship was systematically analyzed by Sayers [J. Phys. D: Appl. Phys. 15 (1982)]. According to Sayers's proposed model, it is possible to construct ultrasonic pole figures via the crystallite orientation distribution function (CODF), which can be derived by using ultrasonic wave velocity changes. In the previous paper, the theoretical modeling to simulate ultrasonic wave velocities propagating in solid materials under plastic deformation has been proposed by the authors and proved to be in good agreement with experimental results. In the present paper, the proposed theoretical modeling is applied to construct the ultrasonic pole figures based upon Sayers's model under various loading conditions of uniaxial tension, pure torsion, equi-biaxial tension-compression, biaxial compression and biaxial tension, respectively. To examine the accuracy and reliability of the ultrasonic pole figures simulated by the proposed theoretical modeling, the ultrasonic pole figures are compared with those analyzed by the finite element polycrystal model (FEPM). The results show a remarkable qualitative similarity among the two methods.

Key Words: Ultrasonic Wave, Pole Figure, Texture, Crystallite Orientation Distribution Function, Finite Element Polycrystal Model, Plastic Deformation

1. Introduction

Many alloys of common metals such as aluminum and steel are polycrystalline aggregates of single crystals having preferred orientation (texture). When a polycrystalline metal is plastically deformed, the crystallites are deformed and rotated due to the crystal slip and partially aligned to a certain crystallographic orientation determined by preferred orientation or texture depending on the plastic flow geometry and magnitude. Generally, the degree and type of texture is most conveniently discussed in terms of the crystallite orientation distribution function (CODF), which gives the probability of a given crystallite in the sample having a specified orientation with respect to the sample axes. Roe[1],[2] and Bunge[3] gave independent, but equivalent methods to obtain CODF based on an expansion of CODF $w(\xi, \phi, \phi)$ in a series of generalized spherical harmonic functions. The quantitative description of the ultrasonic wave velocities represented by the crystallite orientation distribution function (CODF) has been derived by Sayers[4] by adopting Voigt's averaging method to calculate the polycrystalline elastic constants averaged over a polycrystalline aggregate of cubic crystals. More recently, a variety of such techniques has been reported in several review articles and papers by Hirao et al.[5], Clark et al.[6] and Fukuoka et al.[7], where Hirao and Clark presented nondestructive evaluation methods for predicting the anisotropy of the plastic strain ratio (Lankford value or r value), and Fukuoka gave a detailed description of the foundation and application

* Received 12th September, 2002 (No. 00-1203). Japanese original: Trans. Jpn. Soc. Mech. Eng., Vol. 67, No. 658, A (2001), pp. 947-954 (Received 25th September, 2000)

** Department of Mechanical Engineering, Kitami Institute of Technology, 165 Koen-cho, Kitami-shi, Hokkaido 090-8507, Japan. E-mail: kobayasi@stress.mech.kitami-it.ac.jp

of acoustoelasticity. All of them have made a generous contribution to the research work of nondestructive evaluation of texture with ultrasonic waves.

In the authors' previous study, the theoretical modeling of an ultrasonic nondestructive method to evaluate plastically deformed states has been proposed and developed[8)-10)]. Ultrasonic wave velocity changes under uniaxial tension test and combined stress states were studied both theoretically and experimentally[11)-13)]. The good agreement between numerical and experimental results suggested the accuracy of the proposed theoretical modeling. Successively, this method was applied to examine Sayers's model by comparing the simulated results with the experimental data of the longitudinal and transverse wave velocities in both annealed and unannealed aluminum alloy[14)], where an attempt to use Sayers's model to predict texture changes under plastic deformation was also made.

As one in a series of the authors' study on the ultrasonic nondestructive material evaluation method, in this work we apply this method to characterize the texture of 6061 aluminum alloy specimens under various loading conditions of uniaxial tension, pure torsion, equi-biaxial tension-compression, biaxial compression and biaxial tension. The basis of this investigation lies in the relationships between the orientation distribution coefficients and the elastic constants, the latter of which can be determined by ultrasonic wave velocity simulated by the proposed theoretical modeling. To examine the accuracy and reliability of the predicted ultrasonic pole figures, the simulated results are compared with the pole figures analyzed by the finite element polycrystal model (FEPM) proposed by Takahashi[15)].

2. Theoretical Outline

2.1 Plane wave velocities under plastic deformation based upon the proposed theoretical modeling

In order to avoid verbosity and render the whole work self-contained, velocities of the plane waves propagating in a principal direction under plastic deformation are given here directly. The detailed derivation of longitudinal and transverse waves is referred to from previous articles[8)-10)].

Let the coordinate axis x_3 coincide with one of the principal directions of the stresses σ_{ij} and strains ε_{ij} at the predeformed state, and the plane wave propagate in the x_3-direction; then the longitudinal wave velocity V_L and the transverse wave velocities V_{T1} and V_{T2} can be obtained as

$$\rho_0 V_L{}^2=\lambda+2G+\frac{(\lambda+2G)^2}{2G^2}(g_{11}+g_{22}+g_{33})$$
$$-2\left(1+\frac{\lambda}{G}\right)(g_{11}+g_{22})-\frac{4}{9}G^2(\lambda^c_{11}+\lambda^c_{22})-\frac{16}{9}G^2\lambda^c_{33}$$
$$+\left\{5+2\frac{\lambda}{G}-4G(3\lambda+2G)\left(\kappa_2+\frac{2}{3}\kappa_3\right)-\frac{8}{3}G^2\kappa_3\right\}\sigma_3$$
$$-\frac{1}{3}\left\{\frac{6\lambda}{3\lambda+2G}\left(\frac{\lambda}{G}+2\right)+(3\lambda+2G)^2\left(6\kappa_1+3\kappa_2+\frac{2}{3}\kappa_3\right)-4G\lambda(3\kappa_2+2\kappa_3)-\frac{8}{3}G^2\kappa_3\right\}(\sigma_1+\sigma_2+\sigma_3)$$
$$+4(\lambda+2G)[\varepsilon^p_3], \qquad (1)$$

$$\left.\begin{matrix}\rho_0 V_{T1}{}^2\\ \rho_0 V_{T2}{}^2\end{matrix}\right\}=\bar{\Gamma}+\frac{1}{2}\{g_{13}+g_{23}-2G^2(\lambda^c_{13}+\lambda^c_{23})\}$$
$$\pm\left[\Gamma^2+(\Gamma^p)^2+2\Gamma\cdot\Gamma^p\cos 2(\theta-\theta_\varepsilon)+\{g_{13}-g_{23}-2G^2(\lambda^c_{13}-\lambda^c_{23})\}(\Gamma\cos 2\theta+\Gamma^p\cos 2\theta_\varepsilon)+\frac{1}{4}\{g_{13}-g_{23}-2G^2(\lambda^c_{13}-\lambda^c_{23})\}^2\right]^{1/2}, \qquad (2.a, b)$$

in which g_{ij} is inherent anisotropy, ρ_0 is the mass density of the undeformed state, σ_i and ε^p_i are principal stress and principal plastic strain, and θ and θ_ε are the angles between the x_1-axis and the direction of the principal stress and the principal strain, respectively. In Eq.(2), Γ, $\bar{\Gamma}$ and Γ^p are

$$\bar{\Gamma}=G-\left\{\frac{\lambda-2G}{2(3\lambda+2G)}+G^2(2\kappa_2+\kappa_3)\right\}(\sigma_1+\sigma_2+\sigma_3)+\left(\frac{3}{2}-G^2\kappa_3\right)\sigma_3+G[\varepsilon^p_3],$$
$$\Gamma=\left(\frac{1}{2}-G^2\kappa_3\right)(\sigma_1-\sigma_2),\ \Gamma^p=G([\varepsilon^p_1]-[\varepsilon^p_2]),$$

where the detailed expression of λ^c_{ij} and the third-order elastic moduli $\kappa_1\sim\kappa_3$ can be found in previous papers[8)-10)].

2.2 Ultrasonic wave velocities and ultrasonic pole figures in a textured material

2.2.1 Crystallite orientation distribution function The quantitative description of the velocities of ultrasonic wave propagating in the sample requires knowledge of the orientation distribution of crystallites in the sample. Let o-$x_1x_2x_3$ be an orthogonal set of reference axes fixed in the sample with x_1 and x_2 on the plate surface, and x_3 along the wave propagating direction. Let o-$X_1X_2X_3$ be an orthogonal set of axes for a crystallite given by the ⟨100⟩, ⟨010⟩ and ⟨001⟩ crystallographic directions. The orientation of a given crystallite with respect to the sample coordinate system may then be defined uniquely by the three Euler angles θ, ψ and ϕ, as shown in Fig. 1. The crystal coordinate X_i is obtained from the sample coordinate x_i by

(i) a rotation of ψ about ox_3

$$x_1'=x_1\cos\psi+x_2\sin\psi,\ x_2'=-x_1\sin\psi+x_2\cos\psi,\ x_3'=x_3; \qquad (3)$$

(ii) a rotation of θ about ox_2'

$$X_1''=x_1'\cos\theta-x_3'\sin\theta,\ X_2''=x_2',\ X_3''=x_1'\sin\theta+x_3'\cos\theta; \qquad (4)$$

(iii) a rotation of ϕ about oX_3

$$X_1=X_1''\cos\phi+X_2''\sin\phi,\ X_2=-X_1''\sin\phi$$

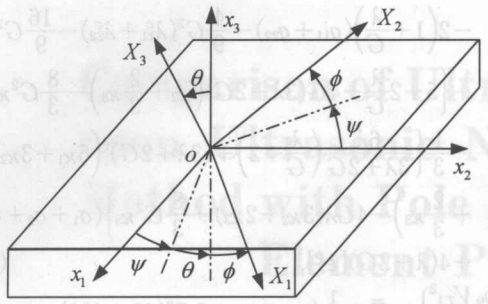

Fig. 1 Coordinate systems of sample and crystals

$$+X_2''\cos\phi,\ X_3=X_3''. \tag{5}$$

Combination of Eqs.(3), (4) and (5) gives

$$\begin{bmatrix}X_1\\X_2\\X_3\end{bmatrix}=\begin{bmatrix}\cos\phi & \sin\phi & 0\\-\sin\phi & \cos\phi & 0\\0 & 0 & 1\end{bmatrix}\begin{bmatrix}\cos\theta & 0 & -\sin\theta\\0 & 1 & 0\\\sin\theta & 0 & \cos\theta\end{bmatrix}\times\begin{bmatrix}\cos\psi & \sin\psi & 0\\-\sin\psi & \cos\psi & 0\\0 & 0 & 1\end{bmatrix}\begin{bmatrix}x_1\\x_2\\x_3\end{bmatrix}. \tag{6}$$

It can be rewritten as

$$X_i=R_{ij}x_j \text{ or } x_i=R_{ji}X_j, \tag{7}$$

where R_{ij} is called transformation matrix, and its components are listed in Table 1.

The orientation distribution of crystallites can be represented by the crystallite orientation distribution function (CODF) $w(\xi,\psi,\phi)$ where $\xi=\cos\theta$. It is convenient to expand CODF as a series. Clearly

$$w(\xi,\psi,\phi)=\sum_{l=0}^{\infty}\sum_{m=-1}^{1}\sum_{n=-1}^{1}W_{lmn}P_l^{mn}(\xi)\times\exp(-im\psi)\exp(-in\phi), \tag{8}$$

where $P_l^{mn}(\xi)$ are the generalized associated Legendre function, and W_{lmn} are the orientation distribution coefficients (ODCs), respectively.

2.2.2 Ultrasonic wave velocities in a textured material The relationships between the elastic constants and ODCs based upon the Voigt averaging methods developed by Sayers[4], and the explicit expressions of ultrasonic wave velocities in anisotropic polycrystalline aggregates in terms of ODCs are reviewed here briefly.

To simplify the problems, it is assumed that the densities of all crystallites in the sample are equal such that the calculation of the ultrasonic wave velocities involves an average over only the single crystal elastic constants. It is also assumed that the polycrystalline aggregate has orthorhombic symmetry, and possesses three orthogonal mirror planes given by the planes x_1x_2, x_2x_3 and x_3x_1, such as a rolled plate. We take a_{ij} as the direction cosines of the crystal frame with respect to the sample frame, then the elastic constants C'_{ijkl} in the sample frame can be expressed in terms of those in the crystal frame C_{ijkl} by

$$C'_{ijkl}=a_{pi}a_{qj}a_{rk}a_{sl}C_{ijkl}, \tag{9}$$

where a_{ij} take the same values as R_{ij}, as listed in Table 1.

Table 1 Components of transformation matrix R_{ij}

	x_1	x_2	x_3
X_1	$\cos\theta\cos\psi\cos\phi-\sin\psi\sin\phi$	$-\cos\theta\cos\psi\sin\phi-\sin\psi\cos\phi$	$\sin\theta\cos\psi$
X_2	$\cos\theta\sin\psi\cos\phi+\cos\psi\sin\phi$	$-\cos\theta\sin\psi\sin\phi+\cos\psi\cos\phi$	$\sin\theta\sin\psi$
X_3	$-\sin\theta\cos\phi$	$\sin\theta\sin\phi$	$\cos\theta$

We adopt the approach of Voigt for averaging the elastic constants and integrate Eq.(9) over Euler angles to yield the clear expressions of C'_{ijkl} as

$$\begin{aligned}
\langle C'_{11}\rangle&=C_{11}-\frac{2}{5}C_\nu-2C_\nu\delta_1\\
\langle C'_{22}\rangle&=C_{11}-\frac{2}{5}C_\nu-2C_\nu\delta_2\\
\langle C'_{33}\rangle&=C_{11}-\frac{2}{5}C_\nu-2C_\nu\delta_3\\
\langle C'_{44}\rangle&=C_{44}+\frac{1}{5}C_\nu+C_\nu\delta_4\\
\langle C'_{55}\rangle&=C_{44}+\frac{1}{5}C_\nu+C_\nu\delta_5\\
\langle C'_{66}\rangle&=C_{44}+\frac{1}{5}C_\nu+C_\nu\delta_6\\
\langle C'_{23}\rangle&=C_{12}+\frac{1}{5}C_\nu+C_\nu\delta_4\\
\langle C'_{31}\rangle&=C_{12}+\frac{1}{5}C_\nu+C_\nu\delta_5\\
\langle C'_{12}\rangle&=C_{12}+\frac{1}{5}C_\nu+C_\nu\delta_6\\
C_\nu&=C_{11}-C_{12}-2C_{44}
\end{aligned} \tag{10}$$

It is pointed out here that it is always convenient to take advantage of the symmetries to represent the fourth-rank tensor C_{ijkl} (or C'_{ijkl}) as a symmetric 6×6 matrix. To convert C_{ijkl} (or C'_{ijkl}) into a two-dimensional matrix, we adopt the convention of Nye[16] and replace the six distinct pairs ij with a single integer m as

Four index tensor indices ij	11	22	33	23, 32	31, 13	12, 21
Two index matrix indices m	1	2	3	4	5	6.

The angular brackets in Eq.(10) indicate an average over all the crystallites in the sample, i.e., an average over the crystalline orientation distribution function $w(\xi,\psi,\phi)$. The symbols $\delta_1,\delta_2,\cdots,\delta_6$ in Eq.(10) take the following forms:

$$\left.\begin{aligned}
\delta_1&=-\frac{6\sqrt{2}}{35}\pi^2\left(W_{400}-\frac{2\sqrt{10}}{3}W_{420}+\frac{\sqrt{70}}{3}W_{440}\right)\\
\delta_2&=-\frac{6\sqrt{2}}{35}\pi^2\left(W_{400}+\frac{2\sqrt{10}}{3}W_{420}+\frac{\sqrt{70}}{3}W_{440}\right)\\
\delta_3&=-\frac{16\sqrt{2}}{35}\pi^2 W_{400}\\
\delta_4&=-\frac{16\sqrt{2}}{35}\pi^2\left(W_{400}+\sqrt{\frac{5}{2}}W_{420}\right)\\
\delta_5&=-\frac{16\sqrt{2}}{35}\pi^2\left(W_{400}-\sqrt{\frac{5}{2}}W_{420}\right)\\
\delta_6&=\frac{4\sqrt{2}}{35}\pi^2(W_{400}-\sqrt{70}W_{420})
\end{aligned}\right\}. \tag{11}$$

Let the coordinate axes of the sample coincide with the directions of principal stresses. For a plane wave propagating in the direction of the x_3 axis at the predeformed state, the longitudinal wave velocity V_L^C and the transverse wave velocities V_{T1}^C, V_{T2}^C are

$$V_L^C=\sqrt{\frac{\langle C'_{33}\rangle}{\rho_0}},\ V_{T1}^C=\sqrt{\frac{\langle C'_{55}\rangle}{\rho_0}},\ V_{T2}^C=\sqrt{\frac{\langle C'_{44}\rangle}{\rho_0}}, \tag{12}$$

where ρ_0 is the density of the sample. If the velocities V_{L0} and V_{T0} in the natural state are expressed in terms of Lamé constants λ and G as ${V_{L0}}^2=(\lambda+2G)/\rho_0$ and ${V_{T0}}^2=G/\rho_0$, respectively, then the explicit formulas for wave velocities propagating in a textured material can be obtainable by combining Eqs.(10)～(12). Clearly

$$\left.\begin{aligned}
\frac{V_L^C}{V_{L0}}&=1+\frac{16\sqrt{2}\pi^2}{35(\lambda+2G)}C_\nu W_{400},\\
\frac{V_{T1}^C}{V_{T0}}&=1-\frac{8\sqrt{2}\pi^2}{35G}C_\nu\left(W_{400}-\sqrt{\frac{5}{2}}W_{420}\right),\\
\frac{V_{T2}^C}{V_{T0}}&=1-\frac{8\sqrt{2}\pi^2}{35G}C_\nu\left(W_{400}+\sqrt{\frac{5}{2}}W_{420}\right).
\end{aligned}\right\} \tag{13}$$

As shown in Eq.(13), substitution of the orientation distribution coefficients W_{400} and W_{420} into Eq.(13) yields longitudinal and transverse wave velocities in textured materials, that is, the ultrasonic wave velocities are dependent upon the ODCs in textured materials. Therefore, it is possible to predict the texture behaviors from ultrasonic wave velocities conversely.

2.2.3 Ultrasonic pole figures Let t specify the normal to a given crystallographic plane, and χ and η denote polar and azimuthal angles between t and axes of sample coordinate system o-$x_1x_2x_3$, as shown in Fig. 2. Roe[2] gave the relationship between the ODCs and the normalized pole intensity $q(\zeta,\eta)(\zeta=\cos\chi)$, that is,

$$q(\zeta,\eta)=\frac{1}{4\pi}+\sum_{l=4}^{\infty}\left\{S_l\sum_{m=0}^{1}P_l^m(\zeta)W_{lm0}\cos m\eta\right\}, \tag{14}$$

where $P_l^m(\zeta)$ is the normalized associated Legendre function. S_l is determined as follows according to different pole figures:

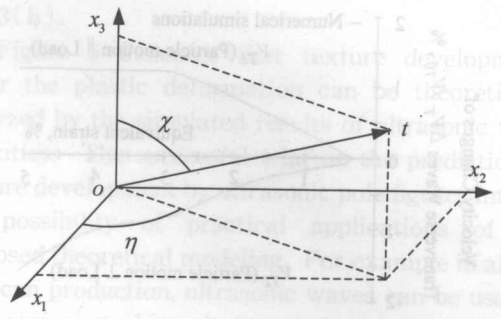

Fig. 2 Orientation of plane normal t with respect to the sample coordinate system o-$x_1x_2x_3$

$$\left.\begin{aligned}
&\langle 100\rangle \text{ pole figure } S_4=2\pi,\ S_6=2\pi,\cdots\\
&\langle 110\rangle \text{ pole figure } S_4=-\pi/2,\ S_6=-13\pi/4,\cdots\\
&\langle 111\rangle \text{ pole figure } S_4=-4\pi/3,\ S_6=32\pi/9,\cdots
\end{aligned}\right\} \tag{15}$$

In the present work, only transverse waves are used to determine W_{400} and W_{420} for calculation of the normalized pole density $q(\zeta,\eta)$ in the $\langle 111\rangle$ pole figure, consequently Eq.(14) is simplified to

$$q(\zeta,\eta)=\frac{1}{4\pi}-\frac{4\pi}{3}\left\{\frac{1}{8}(35\zeta^4-30\zeta^2+3)W_{400}-7.5(7\zeta^4-8\zeta^2+1)W_{420}\cos(2\eta)\right\}. \tag{16}$$

Here, the texture is usually discussed in terms of the ultrasonic pole figure, which is a stereographic projection of the normalized pole density onto a convenient plane. The stereographic projection method will be introduced in the next section.

3. Texture Prediction via Ultrasonic Pole Figures

3.1 Transverse wave velocity changes

In this section, the proposed theoretical modeling of an ultrasonic nondestructive evaluation method is applied to simulate the transverse wave velocity changes under various loading conditions of uniaxial tension (σ_1 : σ_2 : σ_3=1 : 0 : 0), pure torsion (simple shear), equi-biaxial tension-compression (pure shear ; σ_1 : σ_2 : σ_3=1 : −1 : 0), biaxial compression (σ_1 : σ_2 : σ_3=−1 : −1 : 0) and biaxial tension (σ_1 : σ_2 : σ_3=1 : 1 : 0). The transverse wave velocities simulated by Eq.(2) are presented with solid lines in Figs. 3(a)～(c), respectively. Here, we take aluminum 6061-T6 as a study object and the internal state variables used for numerical simulations are those determined by ultrasonic wave velocity measurements with 5 MHz central frequency under uniaxial tension test[13]. We also suppose ultrasonic waves propagating along the x_3-direction. Two modes of transverse wave velocities V_{T1} and V_{T2} in Fig. 3(a)～(c) denote the velocities polarized along the principal directions of stress, respectively, and caused only by plastic deformation without the acoustoelastic effect.

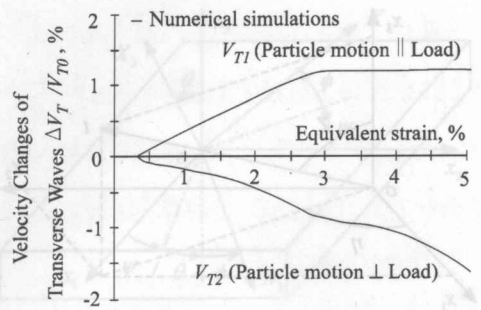

(a) Uniaxial tension

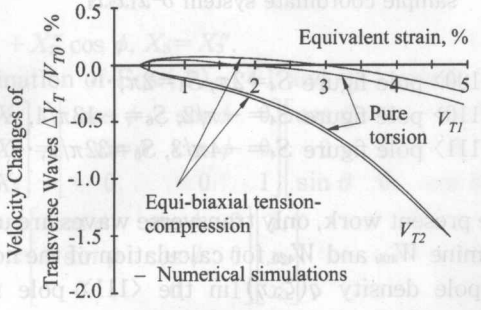

(b) Pure torsion and equi-biaxial tension-compression

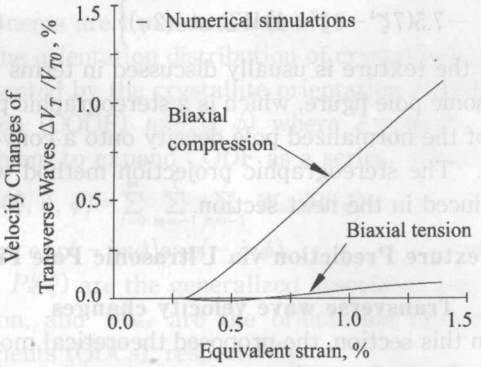

(c) Biaxial compression and biaxial tension

Fig. 3 Velocity changes of transverse waves under uniaxial tension, pure torsion, biaxial tension-compression, biaxial compression and biaxial tension in the plastic deformation range

It can be seen from Fig. 3(a), (b) that velocity changes polarized along the parallel (V_{T1}) and perpendicular (V_{T2}) directions to a principal direction of stress are different from each other with the development of plastic deformation under uniaxial tension, pure torsion and equi-biaxial tension-compression. However, velocity changes of V_{T1} and V_{T2} mutually are overlap under biaxial compression, as so under biaxial tension, as shown in Fig. 3(c). Transverse wave velocity changes under simple and pure shear states illustrated in Fig. 3(b) show nearly the same tendencies with the development of plastic deformation.

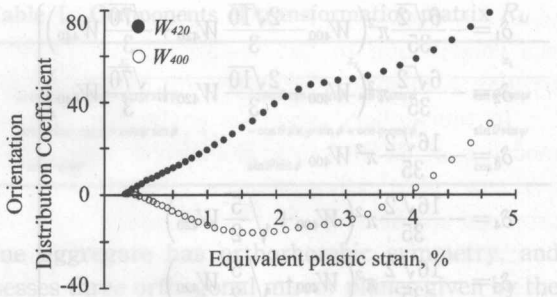

Fig. 4 Orientation distribution coefficient changes under uniaxial tension in the plastic deformation range

3.2 Ultrasonic pole figures

Here in order to avoid verbosity, the uniaxial tension test will be taken as an example to explain how the ultrasonic pole figure is constructed.

First, based upon the numerical results of transverse wave velocities simulated by the proposed theoretical modeling under the uniaxial tension test shown in Fig. 3(a), the orientation distribution coefficients W_{400} and W_{420} are calculated via Eq. (13) as shown in Fig. 4. Here, the hollow and solid circles represent W_{400} and W_{420}, respectively. Next, the normalized pole intensity $q(\zeta, \eta)$ is calculated from the determined ODCs W_{400} and W_{420} at one certain plastic deformation point (for example, at equivalent plastic strain $\bar{\varepsilon}^p = 4.98\%$). Thus, the {111} ultrasonic pole figure can be constructed by projecting the calculated normalized pole density onto the projection plane for the ⟨111⟩ crystallographic direction, as shown in Fig. 5(a).

In the same way, {111} ultrasonic pole figures under the other loading conditions of pure torsion, equi-biaxial tension-compression, biaxial compression and biaxial tension can also be constructed, as shown in Figs. 5(b)～(e), respectively. It should be pointed out here that the longitudinal wave velocity change due to the plastic deformation under pure torsion (simple shear state) is deduced to be zero via theoretical consideration[13], therefore it can be drawn from Eq. (13) that the orientation distribution coefficient W_{400} is also zero. However, velocity changes of a longitudinal wave under equi-biaxial tension-compression (pure shear state) are apparently not equal to zero[13),17], so W_{400} is also not equal to zero according to Eq. (13). This property of W_{400} under simple and pure shear states is responsible for the difference of the ultrasonic pole figures near the central area among both states. However, such a remarkable difference of ultrasonic pole figures under simple and pure shear states is not observed in the outside area except for the 45 degree rotational discrepancy caused by the different loading conditions. This similarity is reflected by the similar transverse wave velocity changes among both states shown in

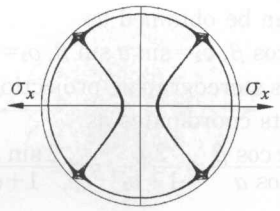

(a) Uniaxial tension: $\bar{\varepsilon}^p=4.98\%$

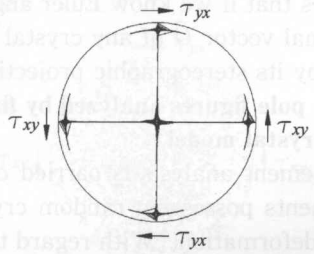

(b) Pure torsion: $\bar{\varepsilon}^p=3.0\%$

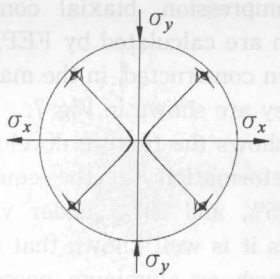

(c) Equi-biaxial tension-compression: $\bar{\varepsilon}^p=4.93\%$

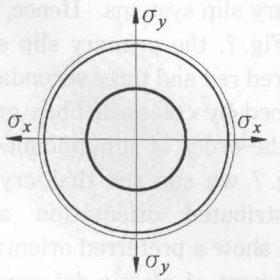

(d) Biaxial tension: $\bar{\varepsilon}^p=1.0\%$

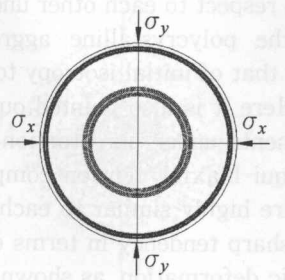

(e) Biaxial compression: $\bar{\varepsilon}^p=1.0\%$

Fig. 5 {111} ultrasonic pole figures of an aluminum alloy based upon ultrasonic nondestructive evaluation method

Fig. 3(b).

Figure 5 indicates that texture developments under the plastic deformation can be theoretically analyzed by the simulated results of ultrasonic wave velocities. The successful trial on the prediction of texture development by ultrasonic pole figures implies the possibility of practical applications of the proposed theoretical modeling. For example in aluminum can production, ultrasonic waves can be used as a process control monitor, namely texture measurement after hot rolling. This appears to be quite promising.

Sayers's theory is based on the following assumptions: the velocities of ultrasonic waves traveling in the (macroscopic) orthotropic continuum are influenced by (1) single crystal moduli and (2) preferred orientation of the crystallites. Other effects, such as grain boundaries, impurities, dislocations, and inhomogeneities are not taken into account in the modeling. Therefore, the accuracy and reliability of the theoretically analyzed results should be compared accordingly with diffraction data of neutrons that penetrate through the metal samples as the ultrasonic waves do. However, the comparison with the neutron diffraction pole figure is not made in the present work, because the neutron equipment is usually available only at some central facilities. The comparison with X-ray diffraction data is also not made here, as X-rays sense only a surface layer on the order of 10 μm thickness. Therefore, an alternative method, i.e., finite element polycrystal model (FEPM) is employed to examine the theoretically analyzed ultrasonic pole figures, because FEPM is already considered as a well-developed technology for the analysis of microstructural behaviors due to plastic deformation.

4. Comparison of Ultrasonic Pole Figures with Pole Figures Analyzed by Finite Element Polycrystal Model

In this section, the finite element polycrystal model (FEPM) proposed by Takahashi[15], where each crystal is regarded as an element and its orientation is given randomly in the case of initial isotropy, is applied to calculate crystal orientations (Euler angles) of face centered cubic (FCC) aggregates under plastic deformation. These calculated Euler angles (θ, ψ, ϕ) are then used to construct {111} pole figures via the stereographic projection method.

4.1 Stereographic projection method

In order to be able to discuss specific directions and planes within a crystal, it is very useful to have some sort of a map on which we can show these directions and planes of crystals. The stereographic projection provides us with such a map and it is widely

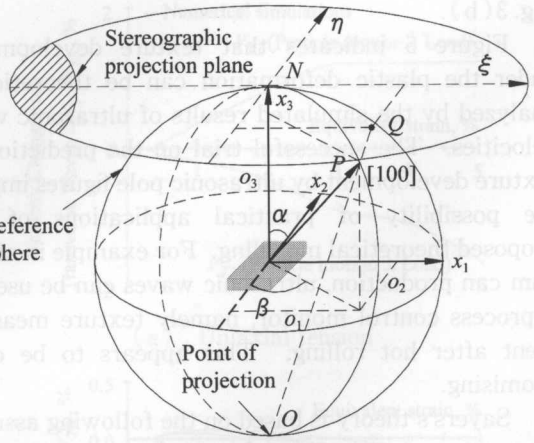

Fig. 6 Schematic diagram of stereographic projection method

used in metallurgical literature. Although extensive information on this subject is available as reported by several authors, for example by John[18], it is still worthwhile to introduce briefly how stereographic projection is obtained.

As is shown in Fig. 6, a sample reference frame is defined first. A reference sphere of unit radius, centered at the origin of the sample reference frame, is then defined. The stereographic projection plane is defined as the tangent plane which comes in contact with the reference sphere at point N in the sample reference frame. In this system, a crystallographic direction, for example, [100], is represented by its pole P at which the direction intersects the reference sphere. The pole P is, then, represented by its stereographic projection Q, which is the intersection of the projection plane with the line OP, where OP is the line from the point of projection O to the pole P.

As discussed in the preceding section, the microscopic coordinate X_i has a relationship with the macroscopic coordinate x_i by Eq.(6) or (7). However, it turns out to be more useful and convenient to specify the orientation of a crystal plane by Miller indices for stereographic projection. Now consider a crystal plane denoted by Miller indices (h_1, h_2, h_3). The cosine directions (O_1, O_2, O_3) of a unit normal vector $\vec{O}$ in this crystal plane can be expressed in terms of Miller indices as

$$O_i=\frac{h_i}{\sqrt{h_1^2+h_2^2+h_3^2}} \quad (i=1, 2, 3). \tag{17}$$

As shown in Fig. 6, the vector $\vec{o}$ with respect to the sample coordinate system is related to the unit normal vector $\vec{O}$ with respect to the crystallite coordinate system, according to Eq.(7), by

$$o_i=R_{ji}O_i \quad (i, j=1, 2, 3). \tag{18}$$

Let the orientation of $\vec{o}$ with respect to the sample coordinate system o-$x_1x_2x_3$ be specified by polar angle α and azimuthal angle β as shown in Fig. 6, then its components can be obtained as

$$o_1=\sin\alpha\cos\beta,\ o_2=\sin\alpha\sin\beta,\ o_3=\cos\alpha. \tag{19}$$

By denoting its stereographic projection as Q, we can easily obtain its coordinates as

$$\xi=\frac{2\sin\alpha\cos\beta}{1+\cos\alpha}=\frac{2o_1}{1+o_3},\ \eta=\frac{2\sin\alpha\sin\beta}{1+\cos\alpha}=\frac{2o_2}{1+o_3}. \tag{20}$$

This indicates that if we know Euler angles (θ, ψ, ϕ), the unit normal vector $\vec{O}$ of any crystal plane can be represented by its stereographic projection.

4.2 {111} pole figures analyzed by finite-element polycrystal model

Finite-element analysis is carried out with $N=9\times9\times9$ elements possessing random crystal orientations before deformation. With regard to the present purpose, Euler angle changes under various loading conditions of uniaxial tension, pure torsion, equi-biaxial tension-compression, biaxial compression, and biaxial tension are calculated by FEPM. {111} Pole figures are then constructed, in the manner described above, and they are shown in Fig. 7.

Figure 7 shows the texture developments due to the plastic deformation (at the equivalent plastic strains 5%, 25% and 50%) under various loading conditions. As it is well known that each crystal in FCC metals such as aluminum possesses four slip planes, the slip system having maximum slip amount among the four slip planes is called primary slip system; the slip systems on the other three planes are called secondary slip systems. Hence, in pole figures, as shown in Fig. 7, the primary slip system in each crystal is colored red and three secondary slip systems are distinguished by colors of blue, green and black according to the order of slip amount.

From Fig. 7 we can see that crystals having a randomly distributed orientation at the initial isotropic state show a preferred orientation according to the development of plastic deformation (25% and 50%). This implies that under the development of plastic deformation, the individual grains will rotate and slide with respect to each other under the applied forces, and the polycrystalline aggregate will be changed from that of initial isotropy to one of strong anisotropy. Here it is also pointed out that the texture developments under pure torsion (simple shear state) and equi-biaxial tension-compression (pure shear state) are highly similar to each other, that is, both show a sharp tendency in terms of the development of plastic deformation, as shown in Figs. 7(b), (c). The discrepancy between the two pole figures lies in the fact that total spin $\dot{\omega}_{12}$ is assumed to be zero under the pure shear state, however, it is clearly not zero under the simple shear state, as expressed by

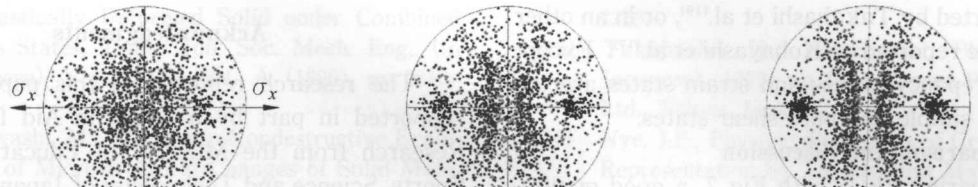

(a) Uniaxial tension

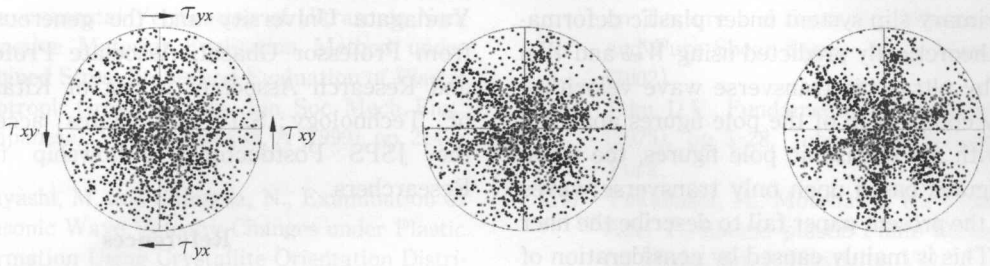

(b) Pure torsion

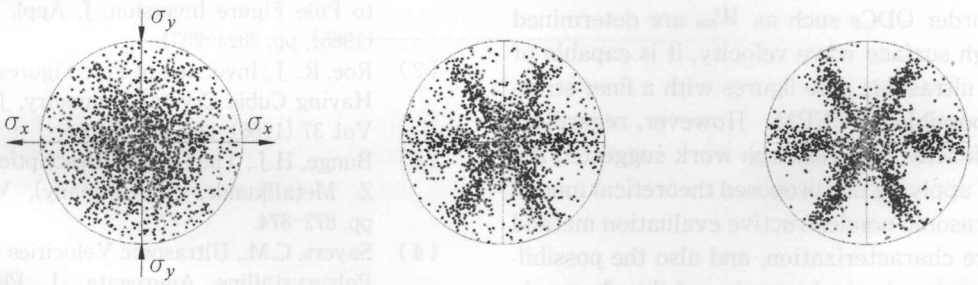

(c) Equi-biaxial tension-compression

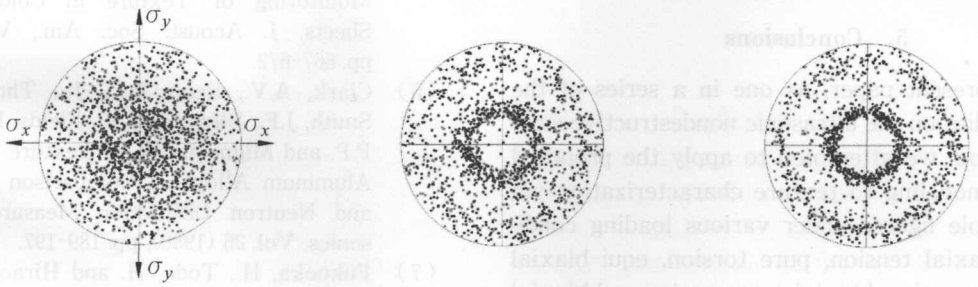

(d) Biaxial tension

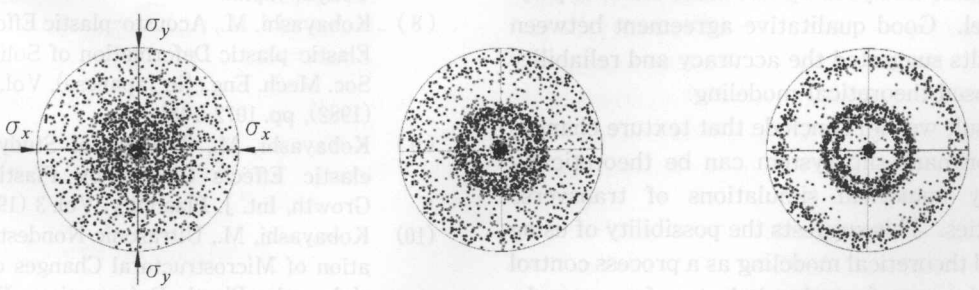

(e) Biaxial compression

$\bar{\varepsilon}^p$=5.0% $\bar{\varepsilon}^p$=25.0% $\bar{\varepsilon}^p$=50.0%

Fig. 7 {111} pole figures in FCC polycrystal analyzed by FEPM

Eq. (25) reported by Takahashi et al.[19], or in an other related article reported by Kobayashi et al.[17]. Except for this discrepancy, stress and strain states are the same among simple and pure shear states.

4.3 Comparison and discussion

By comparing Fig. 5 with Fig. 7, a good qualitative agreement between ultrasonic pole figures and FEPM pole figures of a primary system (denoted by red) is observed. This means that texture development of a primary slip system under plastic deformation can be theoretically predicted using W_{400} and W_{420} determined by ultrasonic transverse wave velocities. However, by comparison of the pole figures analyzed by FEPM with the ultrasonic pole figures, the ultrasonic pole figures based upon only transverse waves presented in the present paper fail to describe the finer structures. This is mainly caused by consideration of only two lower order ODCs to construct ultrasonic pole figures as shown in Eq. (13). In fact, providing that higher order ODCs such as W_{440} are determined from Rayleigh surface wave velocity, it is capable of constructing ultrasonic pole figures with a finer structure[5],[7], as possible by FEPM. However, regardless of such deficiencies, this research work suggested the possibility of applying our proposed theoretical modeling of an ultrasonic nondestructive evaluation method to the texture characterization, and also the possibility of clearing the physical meaning of the ultrasonic pole figure by comparing the ultrasonic pole figures with those analyzed by FEPM.

5. Conclusions

In the present paper, as one in a series of the authors' studies on the ultrasonic nondestructive evaluation method, we attempted to apply the proposed theoretical modeling to texture characterization via ultrasonic pole figures under various loading conditions of uniaxial tension, pure torsion, equi-biaxial tension-compression, biaxial compression and biaxial tension. These predicted results were then compared with pole figures analyzed by the finite element polycrystal model. Good qualitative agreement between the two results suggested the accuracy and reliability of our proposed theoretical modeling.

As a result we can conclude that texture changes caused by primary slip system can be theoretically predicted by numerical simulations of transverse wave velocities. This suggests the possibility of using the proposed theoretical modeling as a process control monitor in the manufacturing industry, for example, texture measurement of a rolled alloy sheet. This appears to be quite promising.

Acknowledgments

The research reported in this paper has been supported in part by a Grant-in-Aid for Scientific Research from the Ministry of Education, Culture, Sports, Science and Technology of Japan under Grant Number 11450039 and Grant Number 2071 (Tokubetsu Kenkyuin Shorei-hi). The authors acknowledge the helpful discussion with Professor Takahashi of Yamagata University and the generous assistance from Professor Ohashi, Associate Professor Fujiki and Research Associate Miura of Kitami Institute of Technology; S.T. appreciates acceptance for the JSPS Postdoctoral Fellowship for Foreign Researchers.

References

(1) Roe, R.-J., Description of Crystallite Orientation in Polycrystalline Materials. III. General Solution to Pole Figure Inversion, J. Appl. Phys., Vol. 36 (1965), pp. 2024-2031.

(2) Roe, R.-J., Inversion of Pole Figures for Materials Having Cubic Crystal Symmetry, J. Appl. Phys., Vol. 37 (1966), pp. 2069-2072.

(3) Bunge, H.J., The General Description on Texture, Z. Metallkunde, (in Germany), Vol. 56 (1965), pp. 872-874.

(4) Sayers, C.M., Ultrasonic Velocities in Anisotropic Polycrystalline Aggregate, J. Phys. D: Appl. Phys., Vol. 15 (1982), pp. 2157-2167.

(5) Hirao, M., Hara, N. and Fukuoka, H., Ultrasonic Monitoring of Texture in Cold-rolled Steel Sheets, J. Acoust. Soc. Am., Vol. 84 (1988), pp. 667-672.

(6) Clark, A.V., Reno, R.C., Jr., Thompson, R.B., Smith, J.F., Blessing, G.V., Fields, R.J., Delsanto, P.P. and Mignogna, R.B., Texture Monitoring in Aluminum Alloys: a Comparison of Ultrasonic and Neutron Diffraction Measurement, Ultrasonics, Vol. 26 (1988), pp. 189-197.

(7) Fukuoka, H., Toda, H. and Hirao, M., Foundations and Applications of Acoustoelasticity, (in Japanese), (1993), pp. 1-195, Ohmsha Press, Tokyo, Japan.

(8) Kobayashi, M., Acousto-plastic Effects Caused by Elastic-plastic Deformation of Solids, Tran. Jpn. Soc. Mech. Eng., (in Japanese), Vol. 48, No. 432, A (1982), pp. 1072-1081.

(9) Kobayashi, M., Theoretical Study of Acousto-elastic Effects Caused by Plastic Anisotropy Growth, Int. J. Plasticity, Vol. 3 (1987), pp. 1-20.

(10) Kobayashi, M., Ultrasonic Nondestructive Evaluation of Microstructural Changes of Solid Materials under Plastic Deformation—Part I, Theory, Int. J. Plasticity, Vol. 14 (1998a), pp. 511-522.

(11) Kobayashi, M., Hatayama, K., Oomori, S., Kubo, T. and Suzuki, T., Ultrasonic Nondestructive Evaluation of Microstructural Property Changes

of Plastically Deformed Solid under Combined Stress States, Trans. Jpn. Soc. Mech. Eng., (in Japanese), Vol. 62, No. 604, A (1996), pp. 2810-2816.

(12) Kobayashi, M., Ultrasonic Nondestructive Evaluation of Microstructural Changes of Solid Materials under Plastic Deformation—Part II, Experiment and Simulation, Int. J. Plasticity, Vol. 14 (1998b), pp. 523-535.

(13) Kobayashi, M., Suzuki, T., Miura, S. and Oomori, S., Experimental Verification of Ultrasonic Nondestructive Material Evaluation Method under Combined Stress States and Evaluation of Plastic Anisotropic Growth, Trans. Jpn. Soc. Mech. Eng., (in Japanese), Vol. 65, No. 638, A (1999), pp. 2149-2156.

(14) Kobayashi, M. and Shimada, N., Examination of Ultrasonic Wave Velocity Changes under Plastic Deformation Using Crystallite Orientation Distribution Function, Trans. Jpn. Soc. Mech. Eng., (in Japanese), Vol. 61, No. 590, A (1995), pp. 2222-2228.

(15) Takahashi, H., Polycrystal Plasticity, (in Japanese), (1999), pp. 1-74, Corona Publishing Co., Ltd., Tokyo, Japan.

(16) Nye, J.F., Physical Properties of Crystals: Their Representation by Tensors and Matrices, (1985), pp. 131-149, Oxford University Press, Oxford.

(17) Kobayashi, M., Tang, S., Miura, S., Iwabuchi, K., Oomori, S. and Fujiki, H., Ultrasonic Nondestructive Material Evaluation Method and Study on Texture and Cross Slip Effects under Simple and Pure Shear States, Int. J. Plasticity, Vol. 19 (2002).

(18) John, D.V., Fundamentals of Physical Metallurgy, (1975), pp. 5-28, John Wiley & Sons, Inc., New York.

(19) Takahashi, H., Motohashi, H., Tokuda, M. and Abe, T., Elastic-plastic Finite Element Polycrystal Model, Int. J. Plasticity, Vol. 10 (1994), pp. 63-80.